Hindawi
Complexity
Volume 2021, Article ID 9948488, 15 pages
https://doi.org/10.1155/2021/9948488

Research Article

Dynamical Analysis and Periodic Solution of a Chaotic System with Coexisting Attractors

Mingshu Chen, Zhen Wang, Xiaojuan Zhang, and Huaigu Tian

Shaanxi International Joint Research Center for Applied Technology of Controllable Neutron Source School of Science, Xijing University, Xi'an 710123, China

Correspondence should be addressed to Zhen Wang; williamchristian@163.com

Received 31 March 2021; Revised 6 June 2021; Accepted 5 August 2021; Published 17 August 2021

Academic Editor: Chong Fu

Chaotic attractors with no equilibria, with an unstable node, and with stable node-focus are presented in this paper. The conservative solutions are investigated by the semianalytical and seminumerical method. Furthermore, multiple coexisting attractors are investigated, and circuit is carried out. To study the system's global structure, dynamics at infinity for this new chaotic system are studied using Poincaré compactification of polynomial vector fields in R^3. Meanwhile, the dynamics near the infinity of the singularities are obtained by reducing the system's dimensions on a Poincaré ball. The averaging theory analyzes the periodic solution's stability or instability that bifurcates from Hopf-zero bifurcation.

1. Introduction

Since the Lorenz system was presented in 1963 [1], many Lorenz-like systems (Shilnikov-type systems) which were associated with saddle-focus have been studied [2–5]. In recent years, many new non-Shilnikov-type chaotic systems have been discovered [6]. These new systems have included any type and number of equilibria or no equilibria [7–10]. And these methods have been applied in image encryption and compression [11–15], identification, and classification of the system [16–18]. The effect of nonlinearity and Hamilton energy on the attractors was studied in [19]. The Hamilton energy feedback [20] can control the dynamics of chameleon chaotic flow. Multistability is an interesting property of chaotic dynamical systems [21]. Coexisting attractors in systems were experimentally observed [22–24], which have more complex hidden characteristics than the ordinary hidden attractors [25]. And these chaotic systems with coexisting attractors have more application value in the fields of memristor chaotic circuit [26–28] and secure communication [29]. Generating many attractors in a programmable system was interesting [30]. The multistability of dual memristive Shinriki oscillator was studied in [29]. In [31], attractor doubling in various dimensions was discussed. The multistability of a 2D sine map was discussed in [32]. In [33], the extreme multistability of a memristive system was investigated.

According to whether the basin of attraction of the chaotic attractor is around the system's equilibrium points, the attractors are called "self-excited attractors" or "hidden attractors." Leonov and Kuznetsov [34] first suggested it. The basin of attraction of a self-excited attractor is around the equilibrium, while in hidden attractors, the basin of attraction does not intersect with any equilibrium points [35]. Hidden attractors were discussed in many dynamics [36, 37]. In [38], the hidden firing of a neuron model was studied. The perpetual points (PPs) were used to find coexisting attractors [39] and determine whether a system is dissipative or not. However, this method was not correct [40]. In some cases, conservative or dissipative attractors can be discovered using the system's algebraic structure. However, in some others, it is dependent on their states, and it should be calculated numerically. Few conservative chaotic systems were reported in [41, 42]. It is a motivation to find the chaotic attractor with "self-excited attractors" coexisting "hidden attractors" or "conservative solutions" coexisting "dissipative solutions." It would be better to give an analytical (or semianalytical and seminumerical) proof of these conservative solutions.

Although many chaotic systems were constructed, many of them have focused on the type of equilibria, simple algebraic structure, the number of equilibria, or specific features in attractors. However, the systems' global dynamics were rarely analyzed. Moreover, the dynamics mainly rely on numerical methods; qualitative analysis is rare. Therefore, it is incredibly interesting to qualitatively analyze the dynamics such as infinity dynamics and periodic solutions. In [43], Sprott proposed three standards (Feasibility of Study, Simple system, and Complex dynamic behavior) for new chaotic systems to be published and used these criteria, and motivated by undiscovered features of systems with coexisting attractors, a following new chaotic system is proposed in this paper:

$$\begin{aligned} \dot{x} &= y, \\ \dot{y} &= -x - yz, \\ \dot{z} &= a - bx^2 + cy^2 + ez. \end{aligned} \tag{1}$$

In comparison with the other well-known chaotic systems, the unique characteristics of the proposed system are as follows. (a) The chaotic system can have an unstable node, a stable node-focus, and no equilibria. (b) The proposed system's chaotic attractor is conservative for some particular parameters but dissipative for others. The conservative nature of the new systems is proved by the semianalytical and seminumerical method. (c) Three coexisting attractors appear in the new system. (d) Infinity dynamics and periodic solutions are analyzed based on Poincaré compactification and the averaging method. Compared with the numerical method, these qualitative analysis methods help understand this new system's global structure.

It can be seen from these characteristics that the new system has rich dynamical properties. Therefore, it is necessary to explore the dynamical properties to analyze the global dynamics. The rest of the paper is organized as follows. In Section 2, chaotic attractors with no equilibria, unstable node, and stable node-focus are presented. The conservative solutions are investigated by four methods: (a) the sum of finite-time local Lyapunov exponents is zero; (b) divergence of the vector field is zero; (c) local Lyapunov dimension is equal to the order of the system; and (d) the Hamiltonian energy of the system is invariable. Furthermore, multiple coexisting attractors and analog circuit simulation are also shown in this section. In Section 3, to research the system's global structure, by reducing the system's dimensions on a Poincaré ball via the theory of Poincaré compactification, the infinity dynamics of the system are obtained. Also, an analytic proof of the existence of the Hopf-zero bifurcation is provided. The periodic solution's stability or instability, born in Hopf-zero bifurcation, is analyzed by the averaging theory in Section 4. Finally, concluding remarks are given in Section 5.

2. Dynamical Analysis

Let $\dot{x} = 0$, $\dot{y} = 0$, and $\dot{z} = 0$; system (1) has a line of equilibria at $(0, 0, z)$ when $a = 0$ and $e = 0$ or has one equilibrium $E(0, 0, (-a/e))$ when $e \neq 0$ or has no equilibrium when $a \neq 0$ and $e = 0$. When $e = 0$, the conservativeness of system (1) can be testified by the divergence as follows:

$$\nabla V = \frac{\partial \dot{x}}{\partial x} + \frac{\partial \dot{y}}{\partial y} + \frac{\partial \dot{z}}{\partial z} = -z(t). \tag{2}$$

The conservativeness is not obvious since the dissipation is given by the time averaged value of $-z(t)$ along the trajectory.

2.1. Chaos in the Studied System (1) with No Equilibrium. System (1) is rotationally symmetric under the transformation $(x, y, z) \longrightarrow (-x, -y, z)$. So, any attractors are either rotationally symmetric around the z-axis or there is a symmetric pair of them. Figure 1 shows the attractors of system (1) with the initial data as $(0, 5, 0)$, the parameters b, c, and e are fixed, and the parameter a is changed ($a = -6.17, a = -4.5$, and $a = -0.8$), using MATLAB R2020b simulation software, and its corresponding attractors with their properties are summarized in Table 1.

Then, calculate the Lyapunov exponents spectrum of system (1) for fixed parameter b, c, and e, and let a varies. When $a \in (-7, 0)$, the local finite-time Lyapunov exponents spectrum and the largest Lyapunov exponent of system (1) are shown in Figure 2.

According to Figure 2, when $a \in (-7, 0)$ and $b = -1, c = 1$, and $e = 0$, the largest Lyapunov exponent trend can be observed. This observation is also verified by Table 1.

Following the definition of average value of the variable $s(t)$ by $\overline{s}(t) = \lim_{t \longrightarrow \infty} (\int_{t_0}^{t} s(t)\mathrm{d}t/t - t_0)$ as stated in Ref. [44], the average of $z(t)$ of system (1) with special parameters is shown in Table 1, system (1) has a conservative solution since the sum of finite-time local Lyapunov exponents is zero, and the average of $z(t)$ of system (1) with special parameters is shown in Figure 3. The plots of average of $z(t)$ are found to be equal to zero as in Figure 3. The results are not shown here to avoid repetition of the figures. The average values of $z(t)$ of the system are zero. In fact, when $b = 0, c = 1$, and $e = 0$, system (1) is a special case of the Nose–Hoover oscillator [45, 46]. It is invariant to the transformation $t \longrightarrow -t$; hence, it is time-reversible with LEs that are symmetric around zero. Furthermore, we can provide a positive definite energy function in a quadratic form as the Hamiltonian function:

$$H = \frac{1}{2}\left(x^2 + y^2 + z^2\right). \tag{3}$$

Taking the time derivative of H, we have

$$\dot{H} = x\dot{x} + y\dot{y} + z\dot{z} = az, \tag{4}$$

which shows that the energy of system (1) is invariable if $\overline{z}(t)$ is zero. Therefore, the system has a conservative nature (in Figure 4(a), see a conservative torus). It also implies that system (1) has coexisting dynamics, which are analyzed in the following section.

2.2. Coexisting Attractors. In Section 2.1, we have seen that system (1) shows chaotic dynamics with no equilibria in $e = 0$. Moreover, since the sum of Lyapunov exponents is

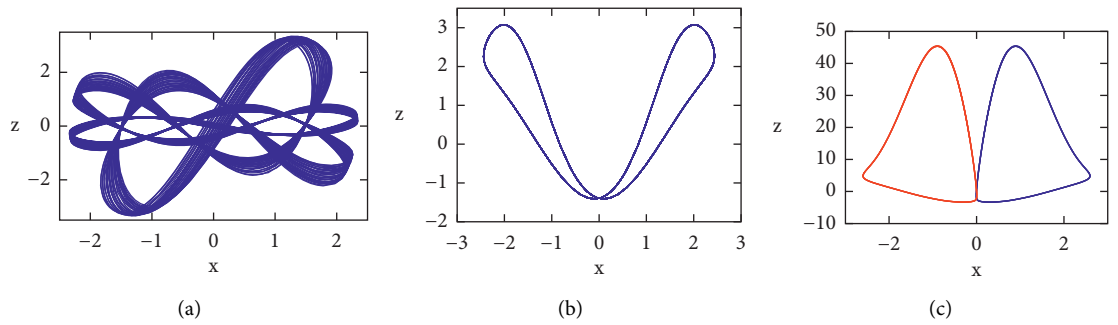

Figure 1: Attractors of system (1) in $b = -1, c = 1$, and $e = 0$ and various values of a: (a) $a = -6.17$; (b) $a = -4.5$; (c) $a = -0.8$.

Table 1: Attractors of system (1) for different values of parameters a and $b = -1, c = 1$, and $e = 0$.

Parameter	Lyapunov exponents	Lyapunov dimension	Attractor type	Phase portrait
$a = -6.17$	[0.003, 0, −0.003]	3	Rotationally symmetric chaotic attractor	Figure 1(a)
$a = -4.5$	[0, −0.37, −0.95]	1	Symmetric limit cycle	Figure 1(b)
$a = -0.8$	[0, −0.02, −26.76]	1	Symmetric pair of limit cycles	Figure 1(c)

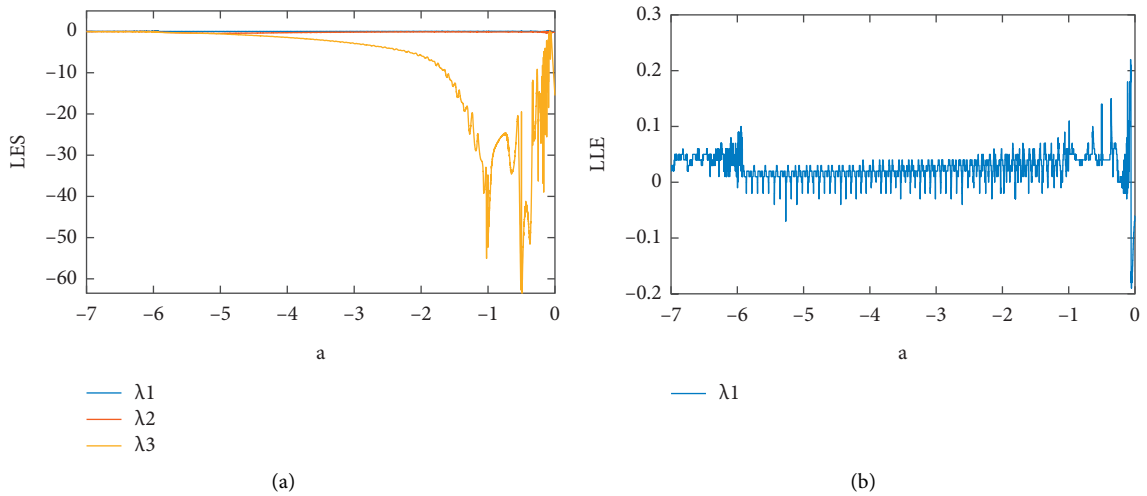

Figure 2: (a) Local finite-time Lyapunov exponents spectrum and (b) largest Lyapunov exponents of system (1) for $b = -1, c = 1, e = 0$, and $a \in (-7, 0)$.

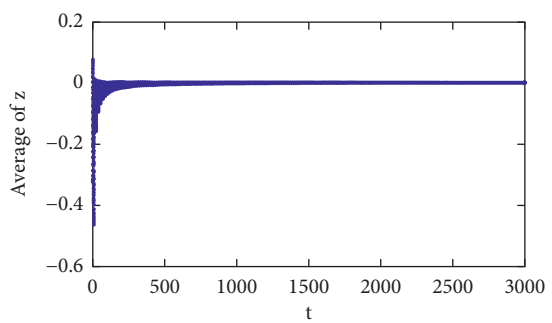

Figure 3: Time averaged value of $z(t)$ for system (1) with $a = -6.17, b = -1, c = 1$, and $e = 0$.

zero for system (1) in special parameters, the conservative solution and chaotic flows are coexisting in this system (in Figure 4(a), chaotic attractor coexists with a torus). Indeed, we can see that there exits a limit cycle for some initial points $a - bx^2 + cy^2 = 0$ and $z = 0$ in $a < 0$, $-b = c = 1$, and $e = 0$. Following these conditions, we can see that if an initial point starts form a limit cycle $x^2 + y^2 = a$ and $z = 0$, we have $\dot{z} = 0$, and the state variable z is fixed. Since $z \equiv 0$, hence, system (1) will become

$$\begin{aligned} \dot{x} &= y, \\ \dot{y} &= -x. \end{aligned} \tag{5}$$

System (5) is a Hamiltonian system (conservative). All orbits start from $x^2 + y^2 = a$ and stay in this circle. So, we claim that system (1) has coexisting attractors under condition $a < 0$, $-b = c = 1$, and $e = 0$. Figure 4 shows some coexisting attractors of system (1) in some special parameter a. Figure 4(b) shows that a chaotic attractor coexists with a limit cycle. Figure 4(c) shows that two limit cycles coexist, and Figure 4(d) shows that three limit cycles (a pair of symmetric limit cycles) coexist.

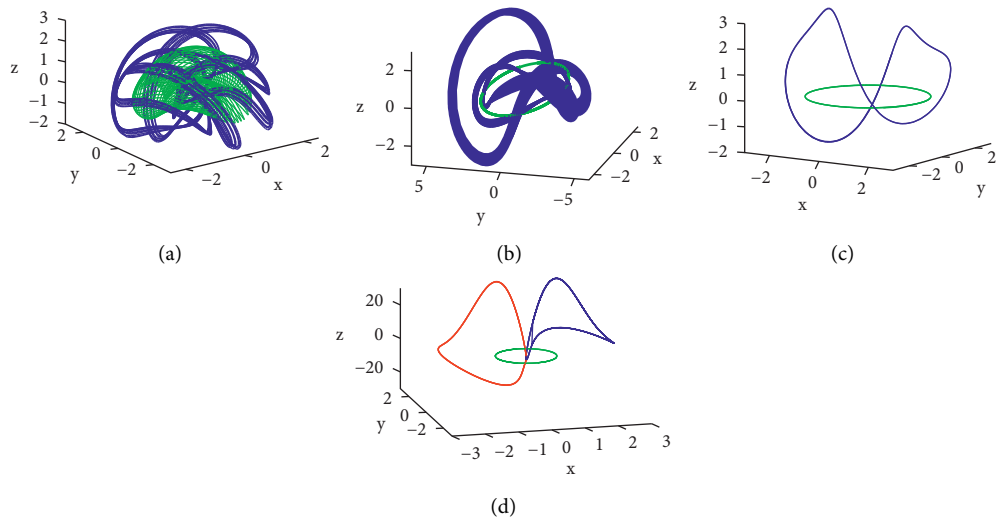

Figure 4: Coexisting attractors of system (1) in $c = 1$ and $e = 0$ at various values of a: (a) chaotic attractor coexists with a torus in system (1) with $a = -1$ and $b = 0$; (b) chaotic attractor coexists with limit cycle in system (1) with $a = -6.17$ and $b = -1$; (c) two limit cycles coexist in system (1) with $a = -4.5$ and $b = -1$; (d) three limit cycles coexist in system (1) with $a = -0.8$ and $b = -1$.

2.3. Chaos in System (1) with One Equilibrium. For the stability of equilibrium, the Jacobian matrix of system (1) is

$$J = \begin{pmatrix} 0 & 1 & 0 \\ -1 & -z & -y \\ -2bx & 2cy & e \end{pmatrix}, \tag{6}$$

and the characteristic polynomial is

$$f = \lambda^3 - (e - z)\lambda^2 - \left(-2cy^2 + ez - 1\right)\lambda - 2bxy - e. \tag{7}$$

The corresponding eigenvalues for equilibrium $E(0, 0, (-a/e))$ are e, $(a \pm \sqrt{a^2 - 4e^2}\,/2e)$. The types of equilibrium for different values of the parameters a and e are summarized in Table 2.

In Table 2, the types of equilibrium under different values of a and e are discussed in two cases of $e > 0$ and $e < 0$, and Tables 3 and 4 show the periodic or chaotic motions for unstable node $(0 < a < 2e)$ and stable node-focus $(0 < a < -2e)$, respectively. The corresponding phase portraits and Poincaré sections are shown in Figures 5 and 6. The Lyapunov exponents spectrum (LES) add largest Lyapunov exponent (LLE) for system (1) versus a are shown in Figure 7.

2.4. Circuit Modeling and Simulation. In this section, the analog circuit is designed in order to illustrate the correctness of system (1). And, according to Section 2.1, fixed $b = -1$, $c = 1$, $e = 0$, system (1) can be rewritten as

$$\begin{cases} \dot{x} = y, \\ \dot{y} = -x - yz, \\ \dot{z} = x^2 + y^2 + a. \end{cases} \tag{8}$$

Then, analog circuit is designed by using LM741 operational amplifiers, AD633 analog multipliers, resistors, and capacitors, where the gain of multiplier AD633 is 0.1 and the power voltage of operational amplifier LM741 is $E = \pm 15$V, and its output saturated voltage is Vsat $\approx \pm 13.5$V. According to system (8), the chaotic circuit is designed, as shown in Figure 8.

Table 2: Types of equilibrium for different values of parameters a and e.

Parameters $(e > 0)$	Type of equilibrium
$0 < 2e < a$	Unstable node
$0 < a < 2e$	Unstable node-focus
$a = 0$	Hopf bifurcation
$2e \le a < 0$	Saddle-focus
$a \le -2e < 0$	Saddle-node
$0 \le -2e < a$	Stable node
$0 \le a < -2e$	Stable node-focus
$a = 0$	Hopf bifurcation
$a \le -2e < 0$	Saddle-node
$2e < a < 0$	Saddle-focus

According to Figure 8 and Kirchhoff's law, the following circuit equation can be obtained:

$$\begin{cases} \dfrac{dx}{dt} = \dfrac{1}{R_0C_0}\left(\dfrac{R}{R_1}y\right), \\ \dfrac{dy}{dt} = \dfrac{1}{R_0C_0}\left(-\dfrac{R}{R_2}x - \dfrac{R}{R_3}yz\right), \\ \dfrac{dz}{dt} = \dfrac{1}{R_0C_0}\left(\dfrac{R}{R_4}x^2 + \dfrac{R}{R_5}y^2 + \dfrac{R}{R_6}a\right). \end{cases} \tag{9}$$

Owing to the limitation of LM741 and AD633 working voltages, the output voltages of the system are reduced to 1/10 of the original. Compress them according to 10: 1, and let time constant $\tau = t/10R_0C_0$, then equation (9) can be expressed as

Table 3: Dynamics of system (1) for different parameter a with $b = 9.5, c = 1$, and $e = 1$ and initial values $[0, 3.9, -0.7]$.

Parameter	Dynamics	Lyapunov exponents	Lyapunov dimension	Phase portrait	Poincaré map
$a = 4.8$	Periodic	[0, −0.01, −0.01]	1	Figure 5(a)	Figure 5(c)
$a = 4.48$	Chaotic	[0.19, 0, −1.06]	2.18	Figure 5(b)	Figure 5(d)

Table 4: Dynamics of system (1) for different parameter a with $b = -0.7, c = -1$, and $e = -1$ and initial values $[0, 0.9, 0]$.

Parameter	Dynamics	Lyapunov exponents	Lyapunov dimension	Phase portrait	Poincaré map
$a = 0.15$	Periodic	[0, −0.01, −0.01]	1	Figure 6(a)	Figure 6(c)
$a = 0.1$	Chaotic	[0.15, 0, −1.37]	2.11	Figure 6(b)	Figure 6(d)

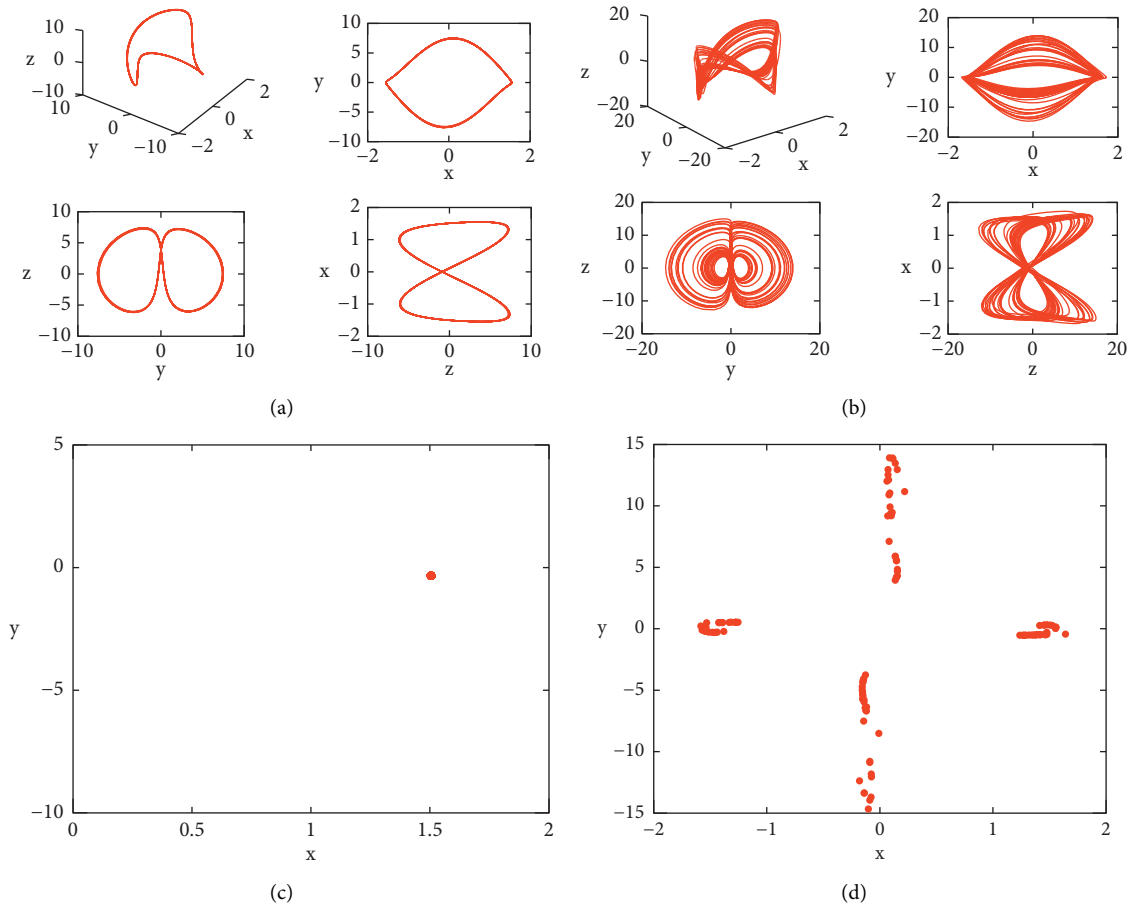

Figure 5: Phase portraits and Poincaré section of system (1) in plane $z = 0$ for some special values of parameter a with constant parameters b, c, and e. (a) Periodic orbit and projection in x-y plane, y-z plane, and z-x plane. (b) Chaotic attractor and projection in x-y plane, y-z plane, and z-x plane. (c) Poincaré section in plane $z = 0$. (d) Poincaré section in plane $z = 0$.

$$\begin{cases} \dfrac{dx}{d\tau} = 10\left(\dfrac{R}{R_1}y\right), \\ \dfrac{dy}{d\tau} = 10\left(-\dfrac{R}{R_2}x - \dfrac{R}{10R_3}yz\right), \\ \dfrac{dz}{d\tau} = 10\left(\dfrac{R}{10R_4}x^2 + \dfrac{R}{10R_5}y^2 + \dfrac{R}{R_6}a\right). \end{cases} \tag{10}$$

In Figure 8, R_0C_0 is the timescale transformation factor. It is found that a better waveform can be observed by adjusting $R_0C_0 = 1 \times 10^{-4}$. At this time, $R_0 = 10\,k\Omega$ and $C_0 = 10$ nF. Let $R = 10\,k\Omega$, from systems (1) and (10), we can get $R_1 = R_2 = R_6 = 100\,k\Omega$ and $R_3 = R_4 = R_5 = 10\,k\Omega$. The circuit simulation experiment results are shown in Figure 9.

From Figure 9, under the different parameters a, the rotationally symmetric chaotic attractor, symmetric limit cycle, and symmetric pair of limit cycles can be observed. Thus, the circuit results are consistent with the numerical results by Figure 1 and Table 1.

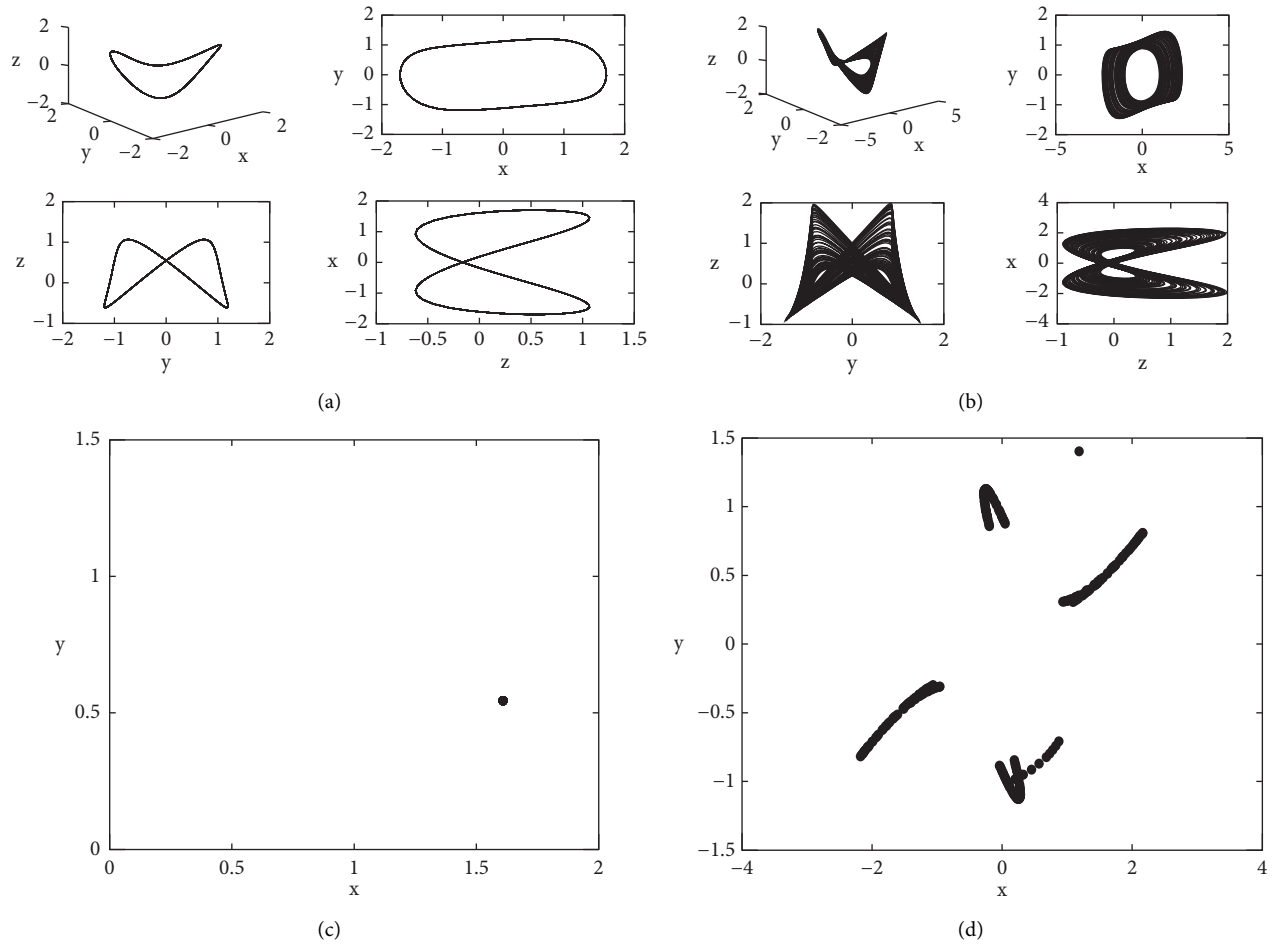

FIGURE 6: Phase portraits and Poincaré section of system (1) in plane $z = 0$ for some special values of parameter a with constant parameters b, c, and e. (a) Periodic orbit and projection in x-y plane, y-z plane, and z-x plane. (b) Chaotic attractor and projection in x-y plane, y-z plane, and z-x plane. (c) Poincaré section in plane $z = 0$. (d) Poincaré section in plane $z = 0$.

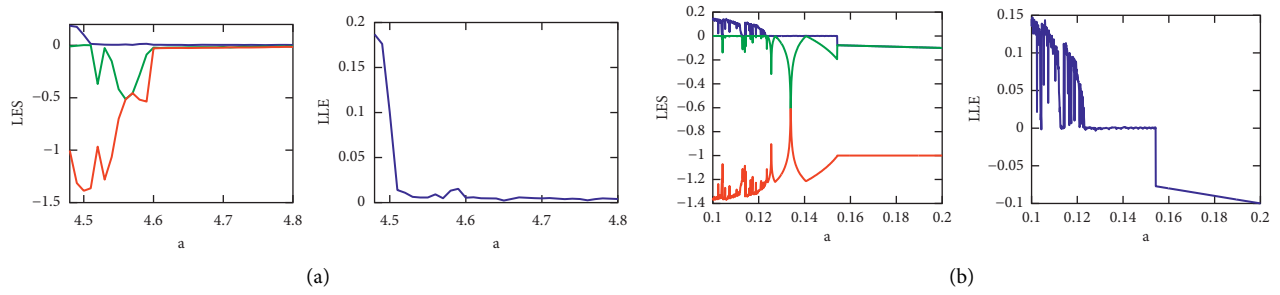

FIGURE 7: Lyapunov exponents spectrum (LES) and largest Lyapunov exponent (LLE) of system (1) versus a. (a) Lyapunov exponents spectrum (LES) and largest Lyapunov exponent (LLE) of system (1) versus a in $b = 9.5$, $c = 1$, and $e = 1$. (b) Lyapunov exponents spectrum (LES) and largest Lyapunov exponent (LLE) of system (1) versus a in $b = 0.7$, $c = 1$, and $e = 1$.

3. Infinity Dynamics

To research the global structure of system (1), we can reduce dimensions of the system on a Poincaré ball by the theory of Poincaré compactification in R^3. So, the behavior of the trajectories of system (1) near infinity can be obtained. Hence, according to the theory of Poincaré Lyapunov compactification [47], let Poincaré ball $S^3 = \{r = (r_1, r_2, r_3, r_4) \in R^4 | \|r\| = 1\}$ be the unit sphere and $S_+ = \{r \in S^3, r_4 > 0\}$ and $S_- = \{r \in S^3, r_4 < 0\}$ be the northern and southern hemisphere. The tangent hyperplanes at the point $(\pm 1, 0, 0, 0)$, $(0, \pm 1, 0, 0)$, $(0, 0, \pm 1, 0)$, and $(0, 0, 0, \pm 1)$ are denoted by the chart U_i and V_i for $i = 1, 2, 3, 4$, where $U_i = \{r \in S^3, r_i > 0\}$ and $V_i = \{r \in S^3, r_i < 0\}$. We only consider the chart U_i and V_i in $i = 1, 2, 3$ for getting the dynamics at x, y, and z infinity.

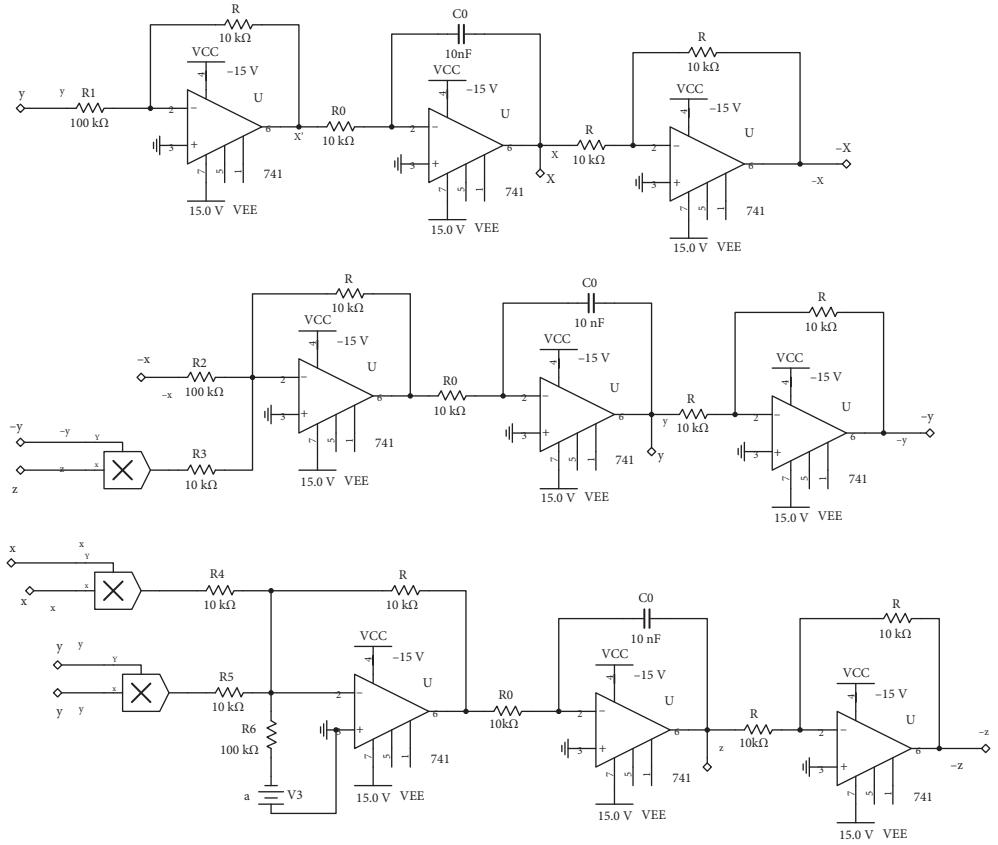

Figure 8: The circuit principle diagram of system (7).

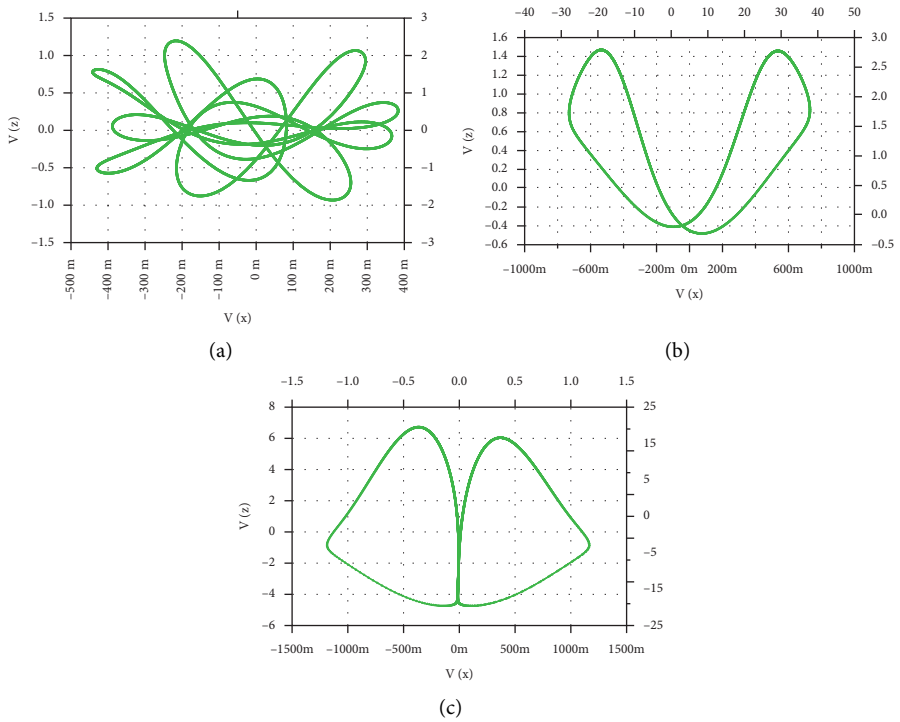

Figure 9: The screenshots of the digital oscilloscope in $x - z$ plane: (a) $a = -6.17$; (b) $a = -4.5$; (c) $a = -0.8$.

In charts U_1 and V_1,take the change of variables $(x, y, z) = (w^{-1}, uw^{-1}, vw^{-1})$ and $t = w\tau$, and system (1) becomes

$$\begin{cases} \dfrac{\mathrm{d}u}{\mathrm{d}\tau} = -u^2 w - uv - w, \\ \dfrac{\mathrm{d}v}{\mathrm{d}\tau} = aw^2 + cu^2 + evw - uvw - b, \\ \dfrac{\mathrm{d}w}{\mathrm{d}\tau} = -uw^2. \end{cases} \tag{11}$$

If $w = 0$, system (11) reduces to

$$\begin{cases} \dfrac{\mathrm{d}u}{\mathrm{d}\tau} = -uv, \\ \dfrac{\mathrm{d}v}{\mathrm{d}\tau} = cu^2 - b. \end{cases} \tag{12}$$

Clearly, we can see that system (12) has two equilibria $(\pm\sqrt{b/c}, 0)$ when $bc > 0$, and no equilibrium when $bc < 0$. Obviously, in $b < 0$ and $c < 0$, the linearized system of (12) has two saddles $(\pm\sqrt{b/c}, 0)$, while the nonlinear system (12) has a same structure as its linearized system. When$b > 0, c > 0$, the linearized system of (12) has two centers $(\pm\sqrt{b/c}, 0)$, and we have the following Proposition 1.

Proposition 1. *When $b > 0$ and $c > 0$, the nonlinear system (12) has two centers $(\pm\sqrt{b/c}, 0)$.*

Proof. Denoting equilibrium $(\pm\sqrt{b/c}, 0)$ as $(u_0, 0)$, we first give a linear transformation:

$$\begin{aligned} u &= \tilde{u} + u_0, \\ v &= \tilde{v}, \end{aligned} \tag{13}$$

and we have

$$\begin{cases} \dfrac{\mathrm{d}\tilde{u}}{\mathrm{d}\tau} = -u_0\tilde{v} - \tilde{u}\tilde{v}, \\ \dfrac{\mathrm{d}\tilde{v}}{\mathrm{d}\tau} = 2cu_0\tilde{u} + c\tilde{u}^2. \end{cases} \tag{14}$$

Let

$$\begin{aligned} \tilde{u} &= \hat{u}, \\ \tilde{v} &= \sqrt{2c}\hat{v}, \end{aligned} \tag{15}$$

we have

$$\begin{cases} \dfrac{\mathrm{d}\hat{u}}{\mathrm{d}\tau} = -\sqrt{2c}\,u_0\hat{v} - \sqrt{2c}\,\hat{u}\hat{v}, \\ \dfrac{\mathrm{d}\hat{v}}{\mathrm{d}\tau} = \sqrt{2c}\,u_0\hat{u} + \dfrac{\sqrt{2c}}{2}\hat{u}^2. \end{cases} \tag{16}$$

Let

$$\begin{aligned} \hat{u} &= r\cos\theta, \\ \hat{v} &= r\sin\theta. \end{aligned} \tag{17}$$

system (17) becomes

$$\begin{cases} \dfrac{\mathrm{d}r}{\mathrm{d}\tau} = -\dfrac{\sqrt{2c}}{2}r^2\cos^2\theta\sin\theta, \\ \dfrac{\mathrm{d}\theta}{\mathrm{d}\tau} = \sqrt{2c}u_0 - \dfrac{\sqrt{2c}}{2}r\left(\cos^3\theta - 2\cos\theta\right). \end{cases} \tag{18}$$

Hence, we have

$$\frac{\mathrm{d}r}{\mathrm{d}\theta} = \frac{-(\sqrt{2c}/2)r^2\cos^2\theta\sin\theta}{\sqrt{2c}u_0 - (\sqrt{2c}/2)r\left(\cos^3\theta - 2\cos\theta\right)} = R_2(\theta)r^2 + R_3(\theta)r^3 + R_4(\theta)r^4 + \cdots. \tag{19}$$

where

$$\begin{cases} R_2(\theta) = -\dfrac{1}{8u_0}(\sin 3\theta + \sin\theta), \\ R_{k+1}(\theta) = \dfrac{R_k(\theta)}{8u_0}(\cos 3\theta - 5\cos\theta) = \dfrac{R_2(\theta)}{(8u_0)^{k-1}}(\cos 3\theta - 5\cos\theta)^{k-1}, \quad k = 2, 3, \ldots. \end{cases} \tag{20}$$

Since $r(\theta) \equiv 0$ for initial conditions $\theta = 0, r = 0$, we suppose that the solution of (19) for a sufficiently small c is

$$r(\theta, c) = r_1(\theta)c + r_2(\theta)c^2 + r_3(\theta)c^3 + \cdots. \tag{21}$$

By the initial condition $r(0, c) = c$, we have

$$\begin{aligned} r_1(0) &= 1, \\ r_k(0) &= 0,\ k = 2, 3, \ldots. \end{aligned} \tag{22}$$

Submitting (21) into system (19), we have

$$\begin{aligned} r_1'(\theta)c + r_2'(\theta)c^2 + r_3'(\theta)c^3 + \cdots = {} & R_2(\theta)\left(r_1(\theta)c + r_2(\theta)c^2 + r_3(\theta)c^3 + \cdots\right)^2 \\ & + R_3(\theta)\left(r_1(\theta)c + r_2(\theta)c^2 + r_3(\theta)c^3 + \cdots\right)^3 + \cdots. \end{aligned} \tag{23}$$

Equating coefficients c, it yields

$$\begin{cases} r_1'(\theta) = 0, \\ r_2'(\theta) = R_2(\theta)r_1^2(\theta), \\ r_3'(\theta) = R_3(\theta)r_1^3(\theta) + 2R_2(\theta)r_1(\theta)r_2(\theta), \\ r_4'(\theta) = R_4(\theta)r_1^4(\theta) + 3R_3(\theta)r_1^2(\theta)r_2(\theta) + R_2(\theta)\left(2r_1(\theta)r_3(\theta) + r_2^2(\theta)\right), \\ \cdots \end{cases} \tag{24}$$

Let

$$\begin{cases} g_2 = \dfrac{1}{2\pi}\displaystyle\int_0^{2\pi} R_2(\theta)r_1^2(\theta)\mathrm{d}\theta, \\ g_3 = \dfrac{1}{2\pi}\displaystyle\int_0^{2\pi} \left(R_3(\theta)r_1^3(\theta) + 2R_2(\theta)r_1(\theta)r_2(\theta)\right)\mathrm{d}\theta, \\ g_4 = \dfrac{1}{2\pi}\displaystyle\int_0^{2\pi} \left(R_4(\theta)r_1^4(\theta) + 3R_3(\theta)r_1^2(\theta)r_2(\theta) + R_2(\theta)\left(2r_1(\theta)r_3(\theta) + r_2^2(\theta)\right)\right)\mathrm{d}\theta, \\ \cdots \end{cases} \tag{25}$$

Noting $\{1, \cos\theta, \sin\theta, \cos 2\theta, \sin 2\theta, \ldots\}$ is an orthonormal basis in a periodic interval $[0, 2\pi]$, by the method of successive function, we can get all $g_k = 0$, $k = 2, 3, 4, \ldots$. Hence, the nonlinear system (12) has two centers $(\pm\sqrt{b/c}, 0)$ when $b > 0$ and $c > 0$. □

Using Poincaré transformation [47], we can get the global phase portraits of system (12) shown in Figure 10 and the following Conclusion 1.

Conclusion 1. (1) When $b > 0$ and $c > 0$, at the positive or negative endpoint of the v axis, it has two semihyperbolic saddles. System (12) has many periodic solutions in the left-half plane and right-half plane (see Figure 10(a)). (2) When $b < 0$ and $c < 0$, system (12) has two saddles $(\pm\sqrt{b/c}, 0)$ and six nodes (three stable nodes and three unstable nodes) at infinity in Poincaré disc. Also, it has eight separatrices which connected two saddles and six nodes at infinity (see Figure 10(b)). (3) When $b < 0$ and $c > 0$, system (12) has one stable node at the positive endpoint of the v axis and one unstable node at the negative endpoint of the v axis (see Figure 10(c)). (4) When v and $c < 0$, system (12) has two semihyperbolic saddles at the positive or negative endpoint of v axis and four nodes (two stable nodes and two unstable nodes) (see Figure 10(d)).

The flow in the chart V_1 is the same as the flow in the chart U_1 reversing the time. Hence, the phase portrait of system (1) on the infinite sphere at the negative endpoint of the x axis is shown in Figure 10, reversing the time direction.

In the charts U_2 and V_2, next we study dynamics of system (1) at infinity of the (HTML translation failed) axis. Taking the transformation $(x, y, z) = (uw^{-1}, w^{-1}, vw^{-1})$ and $t = w\tau$, system (1) becomes

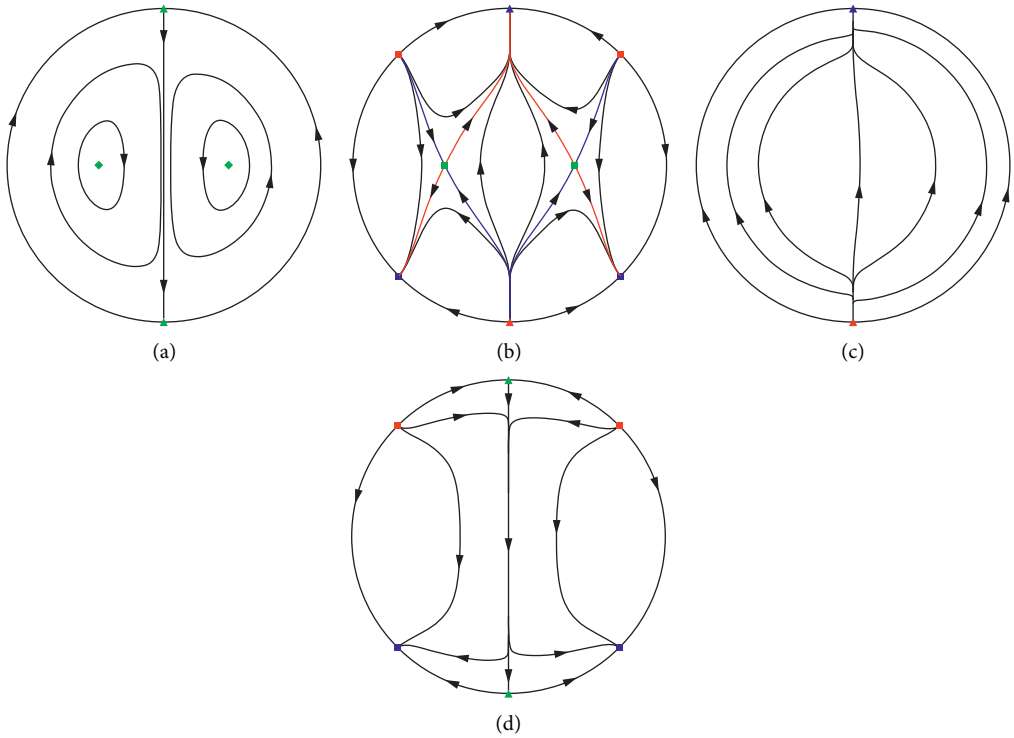

Figure 10: Trajectories in the global phase portraits of system (12). (a) Trajectories in the global phase portraits of system (12) for $b > 0$ and $c > 0$. (b) Trajectories in the global phase portraits of system (12) for $b < 0$ and $c < 0$. (c) Trajectories in the global phase portraits of system (12) for $b < 0$ and $c > 0$. (d) Trajectories in the global phase portraits of system (12) for $b > 0$ and $c < 0$.

$$\begin{cases} \dfrac{du}{d\tau} = u^2 w + uv + w, \\ \dfrac{dv}{d\tau} = aw^2 - bu^2 + evw + uvw + v^2 + c, \\ \dfrac{dw}{d\tau} = uw^2 + vw. \end{cases} \tag{26}$$

If $w = 0$, system (26) reduces to

$$\begin{cases} \dfrac{du}{d\tau} = uv, \\ \dfrac{dv}{d\tau} = -bu^2 + v^2 + c. \end{cases} \tag{27}$$

Clearly, we can see that system (27) has two centers $(\pm\sqrt{c/b}, 0)$ when $b > 0$ and $c > 0$ and one stable node $(0, -\sqrt{-c})$, one unstable node $(0, \sqrt{-c})$, and two saddles $(\pm\sqrt{c/b}, 0)$ when $b < 0$ and $c < 0$. Also, it has one stable node $(0, -\sqrt{-c})$ and one unstable node $(0, \sqrt{-c})$ when $b > 0$ and $c < 0$ and no equilibrium when $b < 0$ and $c > 0$. The corresponding global phase portraits of system (27) are shown in Figure 11.

The flow in the chart V_2 is the same as the flow in the local chart U_2. Hence, the phase portrait of system (1) on the infinite sphere at the negative endpoint of the y axis is shown in Figure 11, reversing the time direction. We can summarize the global behaviors, as shown in 2.

Conclusion 2. (1) When $b > 0$ and $c > 0$, at the positive or negative endpoint of v axis, it has two semihyperbolic saddles. System (27) has many periodic solutions in the left-half plane and right-half plane (see Figure 11(a)). (2) When $b < 0$ and $c < 0$, system (27) has two saddles $(\pm\sqrt{c/b}, 0)$ and two nodes $(0, \pm\sqrt{-c})$ (one is a stable node and the other one is an unstable node) in Poincaré disc. Also, it has two other nodes at the positive and negative endpoint of v axis. Moreover, it has eight separatrices which connect two saddles and four nodes (see Figure 11(b)). (3) When $b < 0$ and $c > 0$, system (27) has one stable node at the positive endpoint of v axis and one unstable node at the negative endpoint of v axis (see Figure 11(c)). (4) When $b > 0$ and $c < 0$, system (27) has two semihyperbolic saddles at the positive or negative endpoint of v axis and two nodes (one stable node and one unstable node) (see Figure 11(d)).

In the charts U_3 and V_3, finally we consider infinity at the z axis. Let $(x, y, z) = (uw^{-1}, vw^{-1}, w^{-1})$ and $t = w\tau$, system (1) becomes

$$\begin{cases} \dfrac{du}{d\tau} = -auw^2 + bu^3 - cuv^2 - euw + vw, \\ \dfrac{dv}{d\tau} = -avw^2 + bu^2 v - cv^3 - evw - uw - v, \\ \dfrac{dw}{d\tau} = -aw^3 + bu^2 w - cv^2 w - ew^2. \end{cases} \tag{28}$$

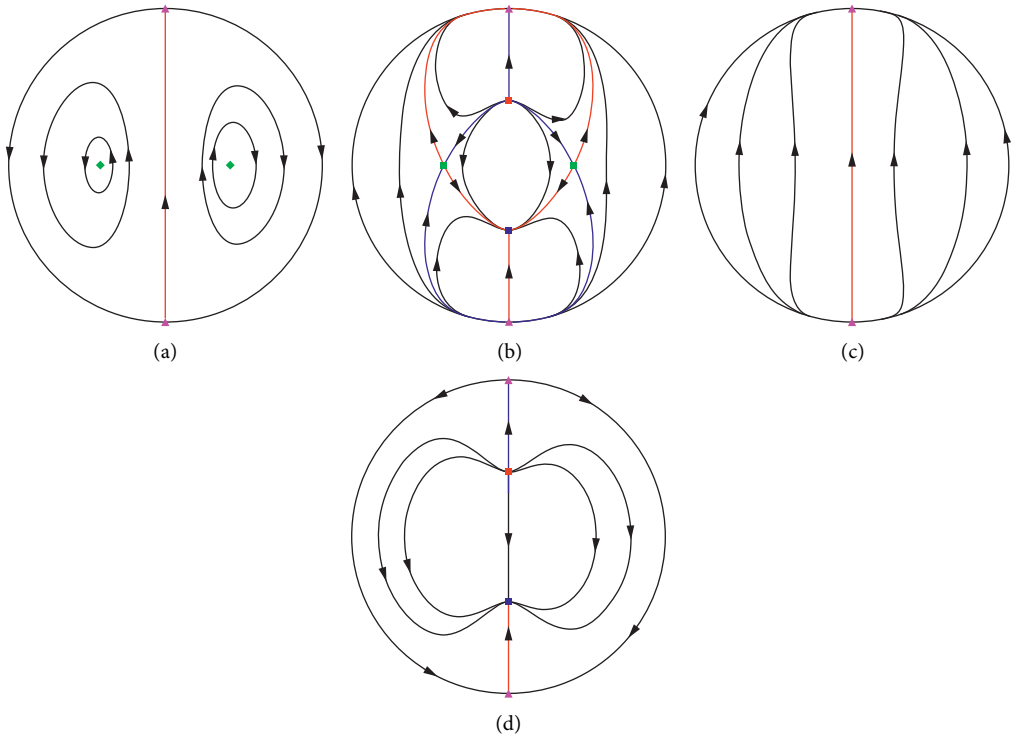

Figure 11: Trajectories in the global phase portraits of system (27). (a) Trajectories in the global phase portraits of system (27) for $b > 0$ and $c > 0$. (b) Trajectories in the global phase portraits of system (27) for $b < 0$ and $c < 0$. (c) Trajectories in the global phase portraits of system (27) for $b < 0$ and $c > 0$. (d) Trajectories in the global phase portraits of system (27) for $b > 0$ and $c < 0$.

If $w = 0$, system (28) reduces to

$$\begin{cases} \dfrac{du}{d\tau} = bu^3 - cuv^2, \\ \dfrac{dv}{d\tau} = bu^2v - cv^3 - v. \end{cases} \tag{29}$$

Clearly, we can see that equation (29) has a saddle $(0, 0)$ when $b < 0$ and $c > 0$ and has one stable node $(0, 0)$ and two unstable nodes $(0, \pm\sqrt{-1/c})$ when $b < 0$ and $c < 0$ and also has one saddle $(0, 0)$ and two unstable nodes $(0, \pm\sqrt{-1/c})$ when $b > 0$ and $c < 0$ and has one stable node $(0, 0)$ when $b < 0$ and $c > 0$. The corresponding global phase portraits of equation (29) are shown in Figure 12.

The flow in the chart V_3 is the same as the flow in the local chart U_3. Hence, the phase portrait of system (1) on the infinite sphere at the negative endpoint of the z axis is shown in Figure 12, reversing the time direction. As in the previous analysis, we can get 3 as follows.

Conclusion 3. (1) When $b > 0$ and $c > 0$, it has a saddle at the origin and four centers at infinity in Poincaré disc (see Figure 12(a)). (2) When $b < 0$ and $c < 0$, system (29) has one stable node $(0, 0)$ and two unstable nodes $(0, \pm\sqrt{-1/c})$. Also, it has four semihyperbolic saddles at infinity in Poincaré disc (see Figure 12(b)). (3) When $b < 0$ and $c > 0$, system (29) has one stable node at origin (see Figure 12(c)). (4) When $b > 0$ and $c < 0$, system (29) has a saddle at the origin and has unstable nodes $(0, \pm\sqrt{-1/c})$ (see Figure 12(d)).

4. Periodic Solution

From Table 2, we can see that system (1) shows Hopf bifurcation at the origin when $a = 0$ and Hopf-zero bifurcation (also called saddle-node Hopf bifurcation or fold Hopf bifurcation) when $a = e = 0$. The Hopf-zero bifurcation can be considered an approximation of Hopf bifurcation when $e \longrightarrow 0$. In this section, we study the Hopf-zero bifurcation at the origin and the periodic orbit, which bifurcates in this bifurcation. Additionally, the stability of this periodic solution will be analyzed. In order to study the periodic solution of system (1), we first introduce averaging theory [48–50].

Lemma 1. *Give the differential equation in the standard form as follows:*

$$\dot{x} = \varepsilon F_1(t, x) + \varepsilon^2 F_2(t, x, \varepsilon), \quad x(0) = x_0, \tag{30}$$

and $x \in D$, where D is an open subset of R^n, $t \geq 0$, $\varepsilon \in (0, \varepsilon_0]$. Moreover, suppose $F_1(t, x)$ and $F_2(t, x, \varepsilon)$ are T periodic in t. Consider the averaged differential equation in D.

$$\dot{y} = \varepsilon f_1(y), \quad y(0) = y_0, \tag{31}$$

where $f_1(y) = (1/T)\int_0^T F_1(t, y)dt$. Assume that

(1) F_1, its Jacobian $\partial F_1/\partial x$, its Hessian $\partial^2 F_1/\partial x^2$, F_2, and its Jacobian $\partial F_2/\partial x$ are continuous and bounded by a constant independent of ε in $[0, \infty] \times D \times (0, \varepsilon_0)$ and $y \in D$ for $t \in [0, 1/\varepsilon]$.

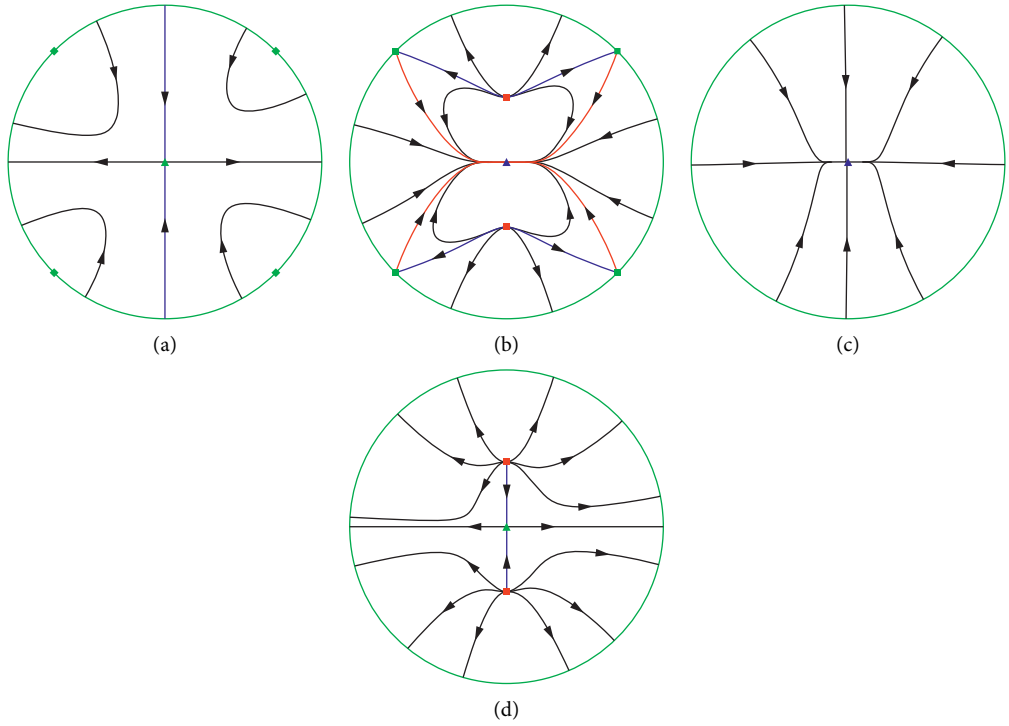

FIGURE 12: Trajectories in the global phase portraits of system (29). (a) Trajectories in the global phase portraits of system (29) for $b > 0$ and $c > 0$. (b) Trajectories in the global phase portraits of system (29) for $b < 0$ and $c < 0$. (c) Trajectories in the global phase portraits of system (28) for $b < 0$ and $c > 0$. (d) Trajectories in the global phase portraits of system (29) for $b > 0$ and $c < 0$.

(2) F_1 and F_2 are T periodic in t (T independent of ε). Then, the following statements hold:

(1) For $t \in [0, 1/\varepsilon]$, we have $x - y = O(\varepsilon)$ as $\varepsilon \longrightarrow 0$.

(2) If p is an equilibrium point of the averaged equation (31) and $\det(\partial_{f1}/\partial_y)|_{y=p} \neq 0$, then there exists a T periodic solution$\varphi(t, \varepsilon)$ of equation (30) such that $\varphi(0, \varepsilon) \longrightarrow p$ as $\varepsilon \longrightarrow 0$.

(3) If the eigenvalues of the equilibrium point p have negative real parts, the corresponding periodic orbit $\varphi(t, \varepsilon)$ is asymptotically stable for sufficiently small ε. If one of the eigenvalues has positive real part, then $\varphi(t, \varepsilon)$ is unstable.

Theorem 1. *System (1) has a Hopf-zero bifurcation at the equilibrium point localized at origin of coordinates when $a = e = 0$. For $a > 0$ sufficiently small, the following statements hold:*

(1) System (1) has two periodic solutions $\gamma_\pm = \{x_\pm(t, a), y_\pm(t, a), z_\pm(t, a)\}$ with period approximately 2π of the form as follows:

$$\begin{aligned} x_\pm(t, a) &= O(a), \\ y_\pm(t, a) &= O(a), \\ z_\pm(t, a) &= -\frac{\sqrt{a}}{2\widetilde{e}} + O(a). \end{aligned} \tag{32}$$

The periodic solution γ_+ has a 3D unstable manifold (a generalized cylinder). Also, the periodic solution γ_- has a 3D stable manifold (a generalized cylinder).

(2) If $b > c$, system (1) has a periodic solution $\varphi(x(t, a), y(t, a), z(t, a))$ with period approximately 2π of the form as follows:

$$\begin{aligned} x^2(t) + y^2(t) &= \frac{a}{b - c} + O(a), \\ z(t) &= O(a). \end{aligned} \tag{33}$$

The solution φ is a linearly stable periodic solution.

Proof. Writing equation (1) in cylindrical coordinates (r, θ, ω) and let

$$\begin{aligned} x &= r\cos\theta, \\ y &= r\sin\theta, \\ z &= w, \end{aligned} \tag{34}$$

we get

$$\begin{aligned} \dot{r} &= -rw\sin^2\theta, \\ \dot{\theta} &= -1 - w\cos\theta\sin\theta, \\ \dot{w} &= a + cr^2\sin^2\theta - br^2\cos^2\theta + ew. \end{aligned} \tag{35}$$

Doing the rescaling of the variables through the changes of coordinates

$$\begin{aligned} r &= \sqrt{a}R, \\ w &= \sqrt{a}W, \\ e &= \sqrt{a}\widetilde{e}, \end{aligned} \tag{36}$$

we have

$$\begin{aligned} \dot{R} &= -\sqrt{a}RW\sin^2\theta, \\ \dot{\theta} &= -1 - \sqrt{a}W\cos\theta\sin\theta, \\ \dot{W} &= \sqrt{a}\left(1 + cR^2\sin^2\theta - bR^2\cos^2\theta + \widetilde{e}W\right). \end{aligned} \tag{37}$$

Equation (37) can be written as

$$\begin{aligned} \frac{\mathrm{d}R}{\mathrm{d}\theta} &= \sqrt{a}RW\sin^2\theta + O(a), \\ \frac{\mathrm{d}W}{\mathrm{d}\theta} &= \sqrt{a}\left(bR^2\cos^2\theta - 1 - cR^2\sin^2\theta - \widetilde{e}W\right) + O(a). \end{aligned} \tag{38}$$

Using the notation of the averaging theory described in Lemma 1, we have

$$\begin{aligned} t &= \theta, \\ T &= 2\pi, \\ \varepsilon &= \sqrt{a}, \\ x &= \begin{pmatrix} R \\ W \end{pmatrix}, \\ F_1(t,x) &= F_1(\theta,R,W) = \begin{pmatrix} F_{11}(\theta,R,W) \\ F_{12}(\theta,R,W) \end{pmatrix}, \\ \varepsilon^2 F_2(t,x) &= O(a), \end{aligned} \tag{39}$$

where

$$\begin{aligned} F_{11}(\theta,R,W) &= RW\sin^2\theta, \\ F_{12}(\theta,R,W) &= bR^2\cos^2\theta - 1 - cR^2\sin^2\theta - \widetilde{e}W. \end{aligned} \tag{40}$$

We can immediately check that equation (38) satisfies the assumptions of Lemma 1, compute the averaged differential equation (30) with $y = (R,W)$, and denote

$$f_1(y) = f_1(R,W) = \begin{pmatrix} f_{11}(R,W) \\ f_{12}(R,W) \end{pmatrix}, \tag{41}$$

where

$$\begin{aligned} f_{11}(R,W) &= \frac{1}{2}RW, \\ f_{12}(R,W) &= \frac{1}{2}\left(bR^2 - cR^2 - 2\widetilde{e}W - 2\right). \end{aligned} \tag{42}$$

Since $f_{11} \equiv 0$, we have the real solutions $(R,W) = (0,-(1/2\widetilde{e}))$ and $(R,W) = (1/\sqrt{b-c},0)$ for $b > c$. The determinant of Jacobian is

$$\det\left(\frac{\partial f_1}{\partial y}\right)\Big|_{y=(R,W)} = \det\begin{pmatrix} \frac{1}{2}W & \frac{1}{2}R \\ (b-c)R & -\widetilde{e} \end{pmatrix}\Big|_{y=(R,W)} = -\widetilde{e}W - \frac{b-c}{2}R^2 = \begin{cases} \frac{1}{2}, & (R,W) = \left(0,-\frac{1}{2\widetilde{e}}\right), \\ -\frac{1}{2}, & (R,W) = \left(\frac{1}{\sqrt{b-c}},0\right), \end{cases} \neq 0. \tag{43}$$

By Lemma 1, for any $a > 0$ sufficiently small, system (37) has a periodic solution $x(t,\varepsilon) = (R(\theta,\sqrt{a}), W(\theta,\sqrt{a}))$ such that $(R(0,\sqrt{a}), W(0,\sqrt{a}))$ tends to $(0,-(1/2\widetilde{e}))$ or $(1/\sqrt{b-c},0)$ for $b > c$ when a tends to 0. The eigenvalues of the Jacobian matrix at the solution $(0,-(1/2\widetilde{e}))$ are $-(1/4\widetilde{e})$, $-\widetilde{e}$. So, the periodic orbit has three stable manifolds when $e > 0$ or three unstable manifolds when $e < 0$. The eigenvalues of the Jacobian matrix at the solution $(1/\sqrt{b-c},0)$ are $-(\widetilde{e}/2) \pm \sqrt{\widetilde{e}^2 + 2}/2$. This shows that the periodic orbit has a 3D stable manifold (a generalized cylinder) and two 2D invariant manifolds (one stable and one unstable, both being cylinders) or a 3D unstable manifold (a generalized cylinder) and two 2D invariant manifolds (one stable and one unstable, both being cylinders).

For $a > 0$ and sufficiently small, going back to the differential system (35), we can get two periodic solutions with period approximately 2π of the form as follows:

$$\begin{aligned} r(\theta) &= O(a), \\ w(\theta) &= -\frac{\sqrt{a}}{2\widetilde{e}} + O(a). \end{aligned} \tag{44}$$

These two periodic solutions of equation (1) become periodic solutions of period close to 2π of the form as follows:

$$x(t) = O(a),$$
$$y(t) = O(a), \tag{45}$$
$$z(t) = -\frac{\sqrt{a}}{2\widetilde{e}} + O(a).$$

These periodic orbits tend to the origin of coordinate when a tends to zero. Therefore, they are small-amplitude periodic solutions starting at the Hopf-zero equilibrium point.

For $a > 0$ sufficiently small and $b > c$, going back to the differential system (35), we can get two periodic solutions with period approximately 2π of the form as follows:

$$r(\theta) = \sqrt{\frac{a}{b-c}} + O(a),$$
$$w(\theta) = O(a). \tag{46}$$

This periodic solution of equation (1) becomes periodic solutions with period close to 2π of the form as follows:

$$x^2(t) + y^2(t) = \frac{a}{b-c} + O(a),$$
$$z(t) = O(a). \tag{47}$$

This periodic orbit tends to the origin of coordinate when a tends to zero. Therefore, it is a small-amplitude periodic solution starting at the Hopf-zero equilibrium point. It completes the proof of Theorem 1. □

5. Conclusion

In this paper, the studied system's chaotic dynamics with no equilibria, with an unstable node, and stable node-focus were provided. Various coexisting attractors were investigated by analytical-numerical methods, and a circuit was carried out, a good similarity between the circuit experimental results and the theoretical analysis was achieved. Furthermore, the infinity dynamics of the system were analyzed using Poincaré–Lyapunov compactification to research the global structure of system. A periodic solution which bifurcates from Hope-zero bifurcation was analyzed by the averaging theory. Indeed, the inner global dynamics and the geometrical structure of this system have been presented entirely. Furthermore, the system was time-reversible with the LEs that were symmetric around zero for some particular parameters. The relations of the time-reversible system and conservative system and the generation mechanism of chaotic dynamics are studied in future works.

Data Availability

All data, models, and code generated or used during the study are included in the submitted article.

Conflicts of Interest

The authors declare that they have no conflicts of interest.

Acknowledgments

This work was supported by the Natural Science Basic Research Program of Shaanxi (2021JM-533, 2021JQ-880, and 2020JM-646), the Innovation Capability Support Program of Shaanxi (2018GHJD-21), the Science and Technology Program of Xi'an (2019218414GXRC020CG021-GXYD20.3), and the Fund of Excellent Doctoral Innovation of Xi 'an University of Technology and the Scientific Research Foundation of Xijing University (XJ21B01).

References

[1] E. N. Lorenz, "Deterministic nonperiodic flow," *Journal of Atoms*, vol. 20, 1963.
[2] T. Ueta and G. Chen, "Yet another chaotic attractor," *International Journal of Bifurcation and Chaos*, vol. 32, 1999.
[3] J. Lu and G. Chen, "A new chaotic attractor coined," *International Journal of Bifurcation and Chaos*, vol. 12, no. 3, pp. 659–661, 2002.
[4] Q. Yang and G. Chen, "A chaotic system with one saddle and two stable node-foci," *International Journal of Bifurcation and Chaos*, vol. 18, no. 5, pp. 1393–1414, 2008.
[5] Z. Wang, S. Baruni, F. Parastesh et al., "Chimeras in an adaptive neuronal network with burst-timing-dependent plasticity," *Neurocomputing*, vol. 406, pp. 117–126, 2020.
[6] S. Jafari, J. C. Sprott, V.-T. Pham, C. Volos, and C. Li, "Simple chaotic 3d flows with surfaces of equilibria," *Nonlinear Dynamics*, vol. 86, no. 2, pp. 1349–1358, 2016.
[7] X. Wang and G. Chen, "A chaotic system with only one stable equilibrium," *Communications in Nonlinear Science and Numerical Simulation*, vol. 17, no. 3, pp. 1264–1272, 2012.
[8] X. Wang and G. Chen, "Constructing a chaotic system with any number of equilibria," *Nonlinear Dynamics*, vol. 71, no. 3, pp. 429–436, 2013.
[9] Z. Wei, "Dynamical behaviors of a chaotic system with no equilibria," *Physics Letters A*, vol. 376, no. 2, pp. 102–108, 2011.
[10] H. Tian, Z. Wang, P. Zhang, M. Chen, and Y. Wang, "Dynamic analysis and robust control of a chaotic system with hidden attractor," *Complexity*, vol. 2021, Article ID 8865522, 9 pages, 2021.
[11] J. Chen, Y. Zhang, L. Qi, C. Fu, and L. Xu, "Exploiting chaos-based compressed sensing and cryptographic algorithm for image encryption and compression," *Optics & Laser Technology*, vol. 99, pp. 238–248, 2018.
[12] Q. Lai, B. Norouzi, and F. Liu, "Dynamic analysis, circuit realization, control design and image encryption application of an extended Lü system with coexisting attractors," *Chaos, Solitons & Fractals*, vol. 114, pp. 230–245, 2018.
[13] E. Tlelo-Cuautle, J. D. Díaz-Muñoz, A. M. González-Zapata et al., "Chaotic image encryption using hopfield and hindmarsh-rose neurons implemented on FPGA," *Sensors*, vol. 20, no. 5, p. 1326, 2020.
[14] A. Silva-Juárez, E. Tlelo-Cuautle, L. Gerardo de la Fraga, and R. Li, "Fpaa-based implementation of fractional-order chaotic oscillators using first-order active filter blocks," *Journal of Advanced Research*, vol. 13, 2020.
[15] O. Guillén-Fernández, M. F. Moreno-López, and E. Tlelo-Cuautle, "Issues on applying one- and multi-step numerical methods to chaotic oscillators for FPGA implementation," *Mathematics*, vol. 9, no. 2, p. 151, 2021.

[16] J. Chen, S. Sun, N. Bao, Z. Zhu, and L.-B. Zhang, "Improved reconstruction for cs based ecg acquisition in internet of medical things," *IEEE Sensors Journal*, vol. 11, 2021.

[17] H. Liang, Z. Wang, Z. Yue, and R. Lu, "Generalized synchronization and control for incommensurate fractional unified chaotic system and applications in secure communication," *Kybernetika*, vol. 48, no. 2, pp. 190–205, 2012.

[18] S. Zhang, C. Zhang, Z. Wang, and W. Kong, "Combining sparse representation and singular value decomposition for plant recognition," *Applied Soft Computing*, vol. 67, pp. 164–171, 2018.

[19] G. Zhang, C. Wang, A. Alsaedi, J. Ma, and G. Ren, "Dependence of hidden attractors on non-linearity and Hamilton energy in a class of chaotic system," *Kybernetika*, vol. 54, no. 4, pp. 648–663, 2018.

[20] F. Wu, T. Hayat, X. An, and J. Ma, "Can Hamilton energy feedback suppress the chameleon chaotic flow?" *Nonlinear Dynamics*, vol. 94, no. 1, pp. 669–677, 2018.

[21] S. Jafari, A. Ahmadi, A. J. M. Khalaf, H. R. Abdolmohammadi, V.-T. Pham, and F. E. Alsaadi, "A new hidden chaotic attractor with extreme multi-stability," *AEU-International Journal of Electronics and Communications*, vol. 89, pp. 131–135, 2018.

[22] Z. Wang, Y. Wu, Y. Li, and Y. Zou, "Adaptive backstepping control of a nonlinear electromechanical system with unknown parameters," *Chaos in Circuits and Systems*, vol. 43, pp. 441–444, 2009.

[23] Z. Wang, I. Moroz, Z. Wei, and H. Ren, "Dynamics at infinity and a hopf bifurcation arising in a quadratic system with coexisting attractors," *Pramana*, vol. 90, no. 1, p. 12, 2018.

[24] Q. Lai, Z. Wan, and P. D. Kamdem Kuate, "Modelling and circuit realisation of a new no-equilibrium chaotic system with hidden attractor and coexisting attractors," *Electronics Letters*, vol. 56, no. 20, pp. 1044–1046, 2020.

[25] Q. Lai, "A unified chaotic system with various coexisting attractors," *International Journal of Bifurcation and Chaos*, vol. 31, no. 01, Article ID 2150013, 2021.

[26] Q. Lai, Z. Wan, P. D. Kamdem Kuate, and H. Fotsin, "Coexisting attractors, circuit implementation and synchronization control of a new chaotic system evolved from the simplest memristor chaotic circuit," *Communications in Nonlinear Science and Numerical Simulation*, vol. 89, Article ID 105341, 2020.

[27] Q. Lai, Z. Wan, and C. Chen, "Two-memristor-based chaotic system with infinite coexisting attractors," *IEEE Transactions on Circuits and Systems II: Express Briefs*, vol. 54, 2020.

[28] L. D. L. F. Esteban Tlelo-Cuautle and J. Rangel-Magdaleno, *Engineering Applications of FPGAs*, Springer, Berlin, Germany, 2016.

[29] Q. Jin, F. Min, and C. Li, "Infinitely many coexisting attractors of a dual memristive shinriki oscillator and its fpga digital implementation," *Chinese Journal of Physics*, vol. 62, pp. 342–357, 2019.

[30] C. Li, W. Joo-Chen Thio, J. C. Sprott, H. H.-C. Iu, and Y. Xu, "Constructing infinitely many attractors in a programmable chaotic circuit," *IEEE Access*, vol. 6, pp. 29003–29012, 2018.

[31] C. Li, T. Lu, G. Chen, and H. Xing, "Doubling the coexisting attractors," *Chaos: An Interdisciplinary Journal of Nonlinear Science*, vol. 29, no. 5, Article ID 051102, 2019.

[32] B. Han, Z. Hua, N. Wang, L. Zhu, M. Chen, and B.-C. Bao, "Initials-boosted coexisting chaos in a 2d sine map and its hardware implementation," *IEEE Transactions on Industrial Informatics*, vol. 18, 2020.

[33] B. Han, M. Chen, H.G. Wu, and B. Bao, "Memristor initial-boosted coexisting plane bifurcations and its extreme multi-stability reconstitution in two-memristor-based dynamical system," *Science China Technological Sciences*, vol. 11, 2019.

[34] G. A. Leonov and N. V. Kuznetsov, *Prediction of Hidden Oscillations Existence in Nonlinear Dynamical Systems: Analytics and Simulation*, Springer International Publishing, Berlin, Germany, 2013.

[35] M.-F. Danca, N. Kuznetsov, and G. Chen, "Unusual dynamics and hidden attractors of the Rabinovich-Fabrikant system," *Nonlinear Dynamics*, vol. 88, no. 1, pp. 791–805, 2017.

[36] M.-F. Danca and N. Kuznetsov, "Hidden chaotic sets in a hopfield neural system," *Chaos, Solitons & Fractals*, vol. 103, pp. 144–150, 2017.

[37] N. V. Kuznetsov, G. A. Leonov, T. N. Mokaev, A. Prasad, and M. D. Shrimali, "Finite-time lyapunov dimension and hidden attractor of the rabinovich system," *Nonlinear Dynamics*, vol. 92, no. 2, pp. 267–285, 2018.

[38] B. Han, A. Hu, W. Liu, and B. Bao, "Hidden bursting firings and bifurcation mechanisms in memristive neuron model with threshold electromagnetic induction," *IEEE Transactions on Neural Networks and Learning Systems*, vol. 31, no. 2, pp. 502–511, 2019.

[39] A. Prasad, "Existence of perpetual points in nonlinear dynamical systems and its applications," *International Journal of Bifurcation and Chaos*, vol. 25, no. 2, Article ID 1530005, 2015.

[40] S. Jafari, F. Nazarimehr, J. C. Sprott, and S. M. R. H. Golpayegani, "Limitation of perpetual points for confirming conservation in dynamical systems," *International Journal of Bifurcation and Chaos*, vol. 25, no. 13, Article ID 1550182, 2015.

[41] H. P. W. Gottlieb and J. C. Sprott, "Simplest driven conservative chaotic oscillator," *Physics Letters A*, vol. 291, no. 6, pp. 385–388, 2001.

[42] H. Jack and F. Zhang, "Nonchaotic and chaotic behavior in three-dimensional quadratic systems: five-one conservative cases," *International Journal of Bifurcation and Chaos*, vol. 17, no. 6, pp. 2049–2072, 2007.

[43] J. C. Sprott, "A proposed standard for the publication of new chaotic systems," *International Journal of Bifurcation and Chaos*, vol. 21, no. 9, pp. 2391–2394, 2011.

[44] Z. Wang, Z. Xu, E. Mliki, A. Akgul, V.-T. Pham, and S. Jafari, "A new chaotic attractor around a pre-located ring," *International Journal of Bifurcation and Chaos*, vol. 27, no. 10, Article ID 1750152, 2017.

[45] S. Nosé, "Constant temperature molecular dynamics methods," *Progress of Theoretical Physics - Supplement*, vol. 103, no. 103, pp. 1–46, 1991.

[46] W. G. Hoover, "Remark on Some simple chaotic flows," *Physical Review E*, vol. 51, no. 1, pp. 759-760, 1995.

[47] F. Dumortier, J. Llibre, and J. Artés, *Qualitative Theory of Planar Differential Systems*, Springer, Berlin, Germany, 2006.

[48] J. Llibre and X. Zhang, "On the hopf-zero bifurcation of the michelson system," *Nonlinear Analysis: Real World Applications*, vol. 12, no. 3, pp. 1650–1653, 2011.

[49] I. A. García, J. Llibre, and S. Maza, "On the periodic orbit bifurcating from a zero hopf bifurcation in systems with two slow and one fast variables," *Applied Mathematics and Computation*, vol. 232, pp. 84–90, 2014.

[50] J. Llibre and C. Valls, "On the integrability and the zero-hopf bifurcation of a chen-wang differential system," *Nonlinear Dynamics*, vol. 80, no. 1, pp. 353–361, 2015.